Hindawi
Geofluids
Volume 2019, Article ID 6402571, 14 pages
https://doi.org/10.1155/2019/6402571

Research Article

The Petrogenesis of the Permian Podong Ultramafic Intrusion in the Tarim Craton, Western China: Constraints from C-He-Ne-Ar Isotopes

Mingjie Zhang,[1] **Pengyu Feng**,[1] **Tong Li**,[1] **Liwu Li**,[2] **Juerong Fu**,[1] **Peng Wang**,[3] **Yuekun Wang**,[1] **Zhongping Li**,[2] **and Xiaodong Wang**[1]

[1]*Key Lab of Mineral Resources in Western China (Gansu), School of Earth Sciences, Lanzhou University, Lanzhou 730000, China*
[2]*Key Lab of Petroleum Resource, Gansu Province, Northwest Institute of Eco-Environment and Resources, CAS, Lanzhou 730000, China*
[3]*Sixth Geological Unit, Xinjiang Bureau of Geology and Mineral Exploration, Hami 839000, China*

Correspondence should be addressed to Mingjie Zhang; mjzhang@lzu.edu.cn

Received 31 March 2019; Revised 26 June 2019; Accepted 10 July 2019; Published 22 August 2019

Academic Editor: Giovanni Martinelli

The Podong Permian ultramafic intrusion is only one ultramafic intrusion with massif Ni-Cu sulfide mineralization in the Pobei layered mafic-ultramafic complex, western China. It is obviously different in sulfide mineralization from the nearby coeval Poyi ultramafic intrusion with the largest disseminated Ni-Cu sulfide mineralization and mantle plume contribution (Zhang et al., 2017). The type and addition mechanism of the confirmed crustal contaminations and possible mantle plume involved in the intrusion formation require evidences from carbon and noble gas isotopic compositions. In the present study, we have measured C, He, Ne, and Ar isotopic compositions of volatiles from magmatic minerals in the Podong ultramafic intrusion. The results show that olivine, pyroxene, and plagioclase minerals in the Podong intrusion have variable $\delta^{13}C$ of CO_2 (-24.5‰ to -3.2‰). The CH_4, C_2H_6, C_3H_8, and C_4H_{10} hydrocarbon gases show normal or partial reversal distribution patterns of carbon isotope with carbon number and light $\delta^{13}C_1$ value of CH_4, indicating the hydrocarbon gases of biogenic origin. The $\delta^{13}C$ of CO_2 and CH_4 suggested the magmatic volatile of the mantle mixed with the volatiles of thermogenic and crustal origins. Carbon and noble gas isotopes indicated that the Podong intrusion could have a different petrogenesis from the Poyi ultramafic intrusion. Two types of contaminated crustal materials can be identified as crustal fluids from subducted altered oceanic crust (AOC) in the lithospheric mantle source and a part of the siliceous crust. The carbon isotopes for different minerals show that magma spent some time crystallizing in a magma chamber during which assimilation of crustal material occurred. Subduction-devolatilization of altered oceanic crust could be the best mechanism that transported large proportion of ASF (air-saturated fluid) and crustal components into the mantle source. The mantle plume existing beneath the Poyi intrusion could provide less contribution of real materials of silicate and fluid components.

1. Introduction

The Pobei Permian mafic-ultramafic complex is the largest layered complex in China and is composed mainly of more than 20 ultramafic intrusions hosting Ni-Cu sulfide mineralization, which intruded in an early-stage large gabbro intrusion [1–6]. These ultramafic intrusions were assumed to be formed by asthenosphere mantle upwelling induced by a mantle plume [1, 6–11] or lithosphere delamination-induced basaltic magmatism in a convergent postcollision tectonic geodynamic setting [2, 12–14]. There is about 10 Ma difference of formation age between early-stage gabbro intrusion and lately ultramafic intrusions [3]; therefore, each ultramafic intrusion could be considered as an individual intrusive event.

The Podong ultramafic intrusion in the Pobei complex is only one ultramafic intrusion with massif Ni-Cu sulfide mineralization [3, 4]. The Podong intrusion is composed

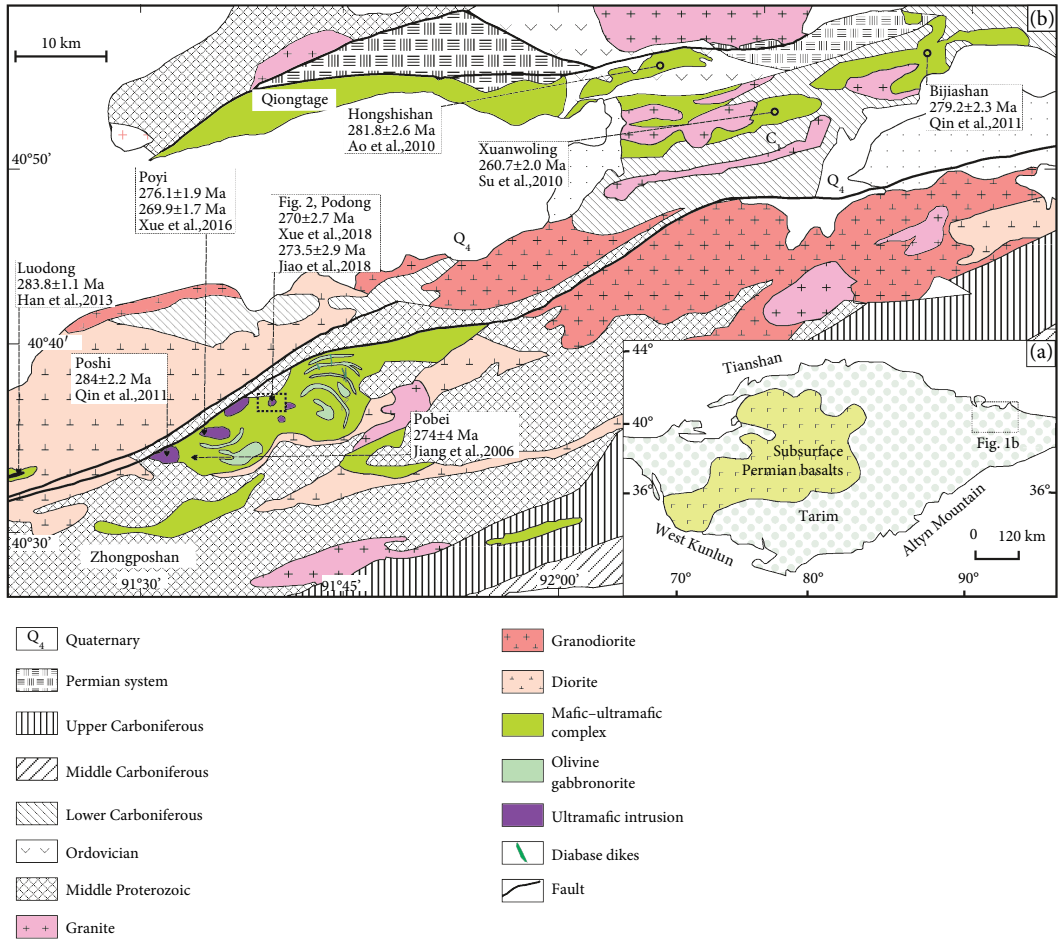

Figure 1: Tectonic (a) and geological sketch maps (b) of mafic-ultramafic complexes in the Beishan area, western China (after [7, 10]).

mainly of lherzolite, websterite, troctolite, gabbro, olivine gabbronorite, and norite, whereas the nearby coeval Poyi (No. 1) ultramafic intrusion contains dunite, wehrlite, troctolite, olivine clinopyroxenite, and olivine gabbro [3, 4]. The Podong Ni-Cu mineralization occurs in gabbronorite (±olivine) with high Ni grade, whereas the Poyi intrusion in the west end of the Pobei complex hosts disseminated sulfide deposit in troctolite and peridotite ultramafic rocks with low Ni grade [4]. The zircon U-Pb age of gabbronorite in the Podong intrusion is 270 ± 2.7 Ma [3] or 273.5 ± 2.9 Ma [4].

The Podong ultramafic intrusion shows pronounced negative anomalies of Nb, Ta, Ti, Zr, and Hf high field strength elements. The external fluids and siliceous crustal assimilations may have triggered sulfide saturation in the mineralization of the Podong magma [3, 4]. The εNd(t) (-0.61–+1.92) and variable $(^{87}Sr/^{86}Sr)_i$ (0.7055–0.7090) indicated that the Podong parental magma experienced 0–13 wt% contamination of the upper crust [3]. However, the 0–13 wt% upper crust suggested by Sr-Nd isotopes which cannot fully account for the negative Nb-Ta anomalies [3, 4]. Meanwhile, the sulfur isotopic compositions (0.82-2.02‰) cannot completely rule out the addition of external sulfur or fluids in the Podong intrusion [3].

On the other hand, the carbon and noble gas isotopic compositions revealed the information of mantle plume in the Poyi ultramafic intrusion [10], but indicated the different petrogenesis of No. 4 and 10 ultramafic intrusions at the west end of the Pobei complex, which showed a mixture of different portion of lithospheric mantle, crust, and air [11]. Hence, the type of contaminated crustal materials and the contribution of the mantle plume in the formation of the Podong intrusion require constraints from C and He-Ne-Ar isotopic compositions. An integrated study of C and He-Ne-Ar isotopes of magmatic minerals in the Podong ultramafic intrusion has been carried out to constrain the origins of volatiles, to reveal the type and mechanism of the contaminated crustal material, and to provide insight into the petrogenesis of the Podong ultramafic intrusion.

2. Geological Background

The Podong ultramafic intrusion is located at the center of the Pobei mafic-ultramafic complex in the northeastern margin of the Tarim Craton, western China. The Pobei complex is associated temporally and spatially with the Cantoushan, Bijiashan, Hongshishan, Xuanwoling, and Zhongposhan mafic-ultramafic complexes in the Beishan Paleozoic rift (Figure 1). These coeval Paleozoic magmatisms were intruded extensively into the Proterozoic and Carboniferous strata and hosted the Ni-Cu-Fe mineralization [2, 5, 6, 15, 16].

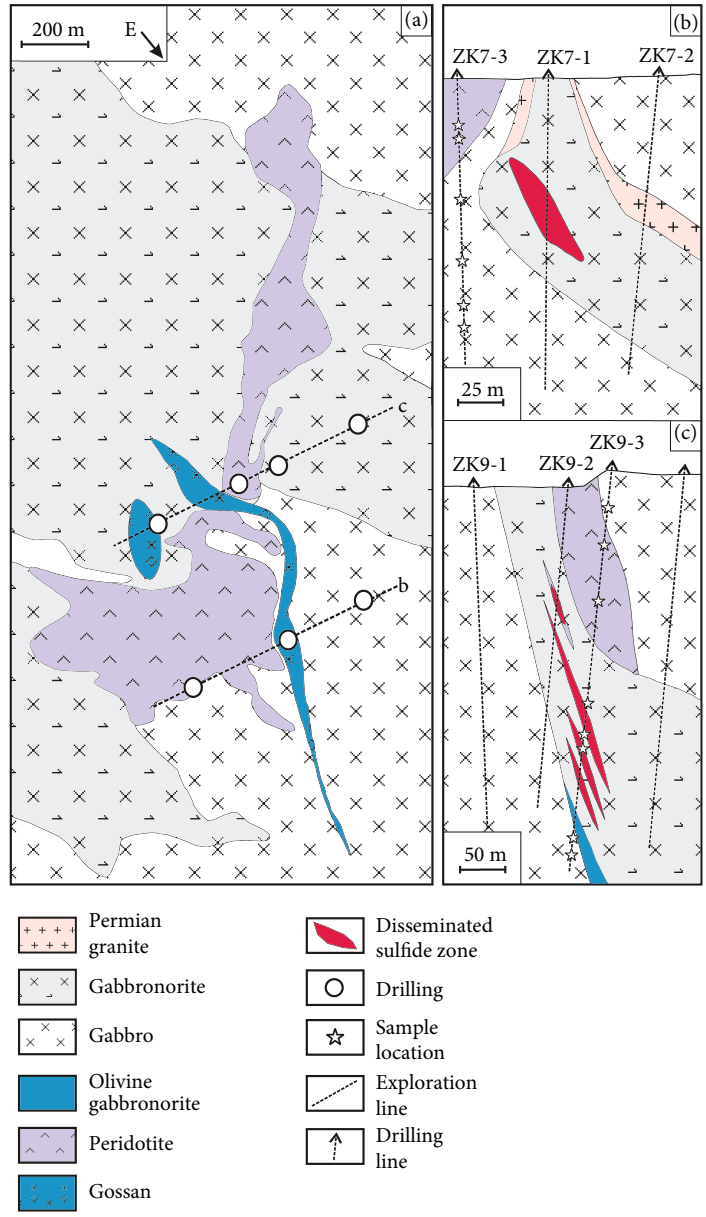

Figure 2: Geological sketch map (a) and vertical cross sections at exploration line 7 (b) and line 9 (c) of the Podong ultramafic intrusion, China (after [4]).

The Pobei mafic-ultramafic complex is ~36 km in length and ~8 km in width on the surface (Figure 1). The downward extension of the intrusion exceeds 2400 m [10]. It is predominantly composed of an early-stage huge gabbroic intrusion intruded by more than 20 small sulfide-mineralized ultramafic-troctolitic intrusions, including Poyi (No. 1), Posan (No. 3), Posi (No. 4), and Poshi (No. 10) ultramafic intrusions [2, 5, 13]. The contacts between the ultramafic-troctolite intrusions and the gabbroic intrusion show clear intrusive relations. Country rocks are Proterozoic schists, gneiss, and gneissic granite (Figure 1).

The ultramafic intrusions are commonly composed of dunite, peridotite, pyroxenite, troctolite, and gabbro with significant cumulate rhythmic layers of magmatic minerals [2, 5, 6, 13, 15, 17]. The contacts among the ultramafic rocks are gradational. The formation ages of the ultramafic intrusions and the early-stage gabbro intrusion are significantly different (Figure 1). The zircon U-Pb isotope ages are 269.9 ± 1.7 Ma for the Poyi ultramafic intrusion [2], 275.8 ± 2.7 Ma for the Posan intrusion [9], and 284.0 ± 2.2 Ma for the Poshi intrusion [1]. The gabbro intrusion has a zircon U-Pb isotope age of 276.1 ± 1.9 Ma [2].

The Podong intrusion surface exposure is ~1400 m in length and 80–400 m in width, with a downward extension > 600 m (Figure 2) [3]. Immediate country rocks are Late Paleozoic gabbros (Figure 2). Many dolerite dykes are present in the south and east of the Podong intrusion and have a zircon U-Pb age of ~280.5 ± 2.0 Ma [2]. Drilling confirmed that Podong Ni-Cu sulfide mineralization formed an economic sulfide deposit as steeply dipping net-texture

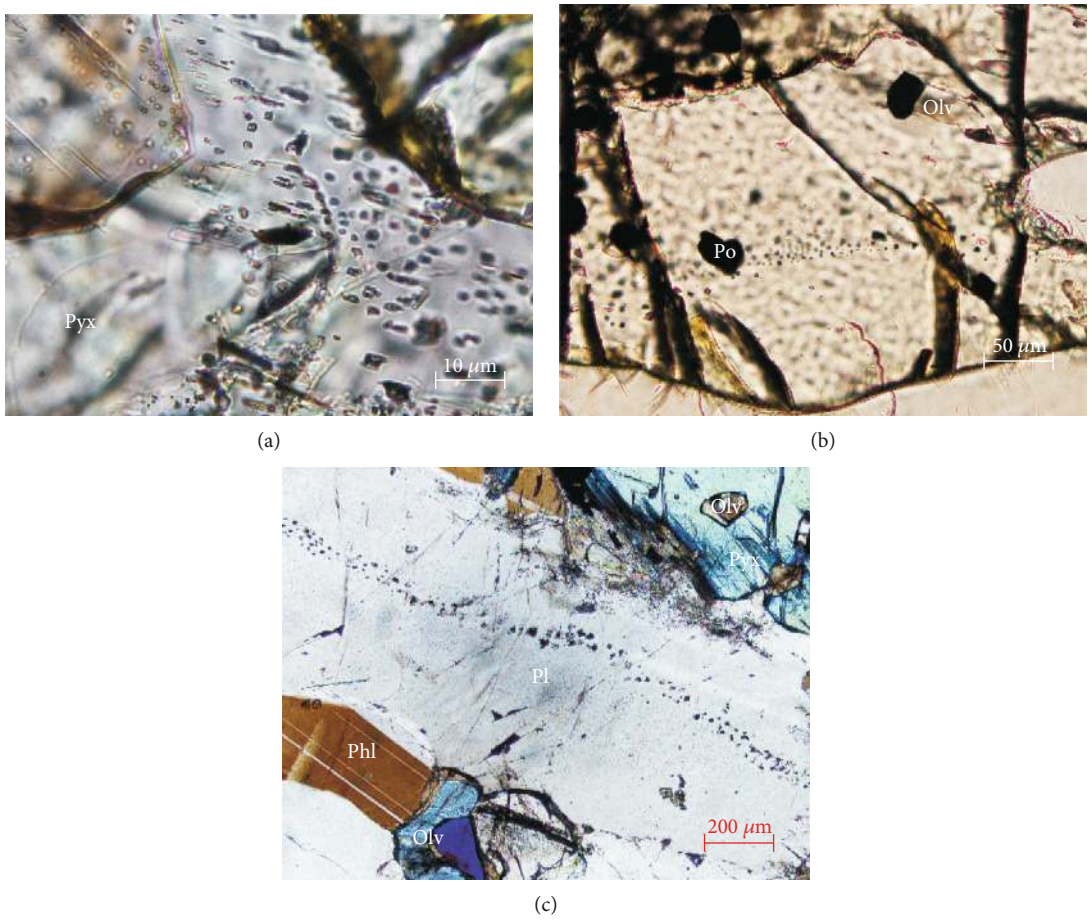

Figure 3: Microphotos of different types of fluid inclusions in the Podong ultramafic intrusion, China. (a) Primary fluid inclusions in pyroxene of sample PD73-1, plane polarized light (-); (b) primary fluid inclusions in olivine of sample PD73-2, plane polarized light (-); (c) secondary fluid inclusions in plagioclase of sample PD73-5, perpendicular polarized light (+). Olv = olivine; Pyx = pyroxene; Pl = plagioclase; Phl = phlogopite; Po = pyrrhotite.

sulfide lenses at lines 7 to 9; Ni-Cu sulfide mineralization is mostly associated with gabbronorite at the center of the intrusion. The sulfide minerals commonly interstitial in the silicate matrix are dominated by pyrrhotite with minor pentlandite and chalcopyrite [3, 4, 18].

3. Sampling and Analytical Methods

3.1. Samples. Twenty-three peridotite, pyroxenite, troctolite, olivine gabbronorite, and gabbro samples used in this study were sampled from three drill cores (ZK7-3, ZK9-3, and ZK11-3) at exploration lines 7, 9, and 11, respectively, in the Podong ultramafic intrusion. The locations of exploration lines with drilled holes are shown in Figure 2, and the representative exploration profiles and sample locations are shown in Figures 2(b) and 2(c). All the rock samples were cut into polished thin sections. The microscopic petrology is observed using both reflected- and transmitted-light microscopy.

The mineral compositions, texture, and other petrographical characteristics of the Podong ultramafic intrusion are reported in reference [3] and are similar to the Poyi intrusion [10]. Olivine, pyroxene, and plagioclase magmatic minerals have different types of fluid inclusions and trapped the volatiles in different stages of magmatism (Figure 3). Partial alteration of olivine by serpentine plus secondary magnetite and clinopyroxene by tremolite are observed in the Podong ultramafic intrusion. Plagioclase is generally pristine, with a negligible alteration in the samples.

3.2. Sample Preparation. All the rock samples were observed using petrography microscopy, and the least altered samples were selected for mineral separation. The rock samples were cut into small pieces. The selected rock pieces without weathered surface, visible secondary veins were crushed and sieved 0.2–0.3 mm in diameter portions. The mineral separates were first of all selected by magnetic separation and followed by hand-picking using a binocular microscope.

The samples for carbon isotopic analysis were immersed in 0.3 M HCl for 24 h and then ultrasonically cleansed with analytical grade CH_2Cl_2, which can remove possible secondary organic components, after which they were rinsed with distilled water until the pH value of the rinsing water reached about 7. The samples for noble gas isotopic analysis were washed with 5% HNO_3 in an ultrasonic bath to remove possible secondary radiogenic components [19].

The cleaned mineral separates were baked at 110°C prior to analysis [10, 20–22].

3.3. Analytical Methods

3.3.1. Carbon Isotope Analysis. Carbon isotopes of CO_2 and CH_4, C_2H_6, C_3H_8, and C_4H_{10} hydrocarbon gases were analyzed by a GC-C-MS system using a stepwise heating extraction procedure. Carbon isotopes are expressed as $\delta^{13}C\,(‰) = ([^{13}C/^{12}C]_{sample}/[^{13}C/^{12}C]_{PDB} - 1) \times 10^3$ (where PDB (Pee Dee Belemnite) is the reference standard). A well-established online stepwise heating method was used for the extraction of volatiles from the magmatic mineral separates [21, 23, 24].

The gas extraction apparatus is composed of a U-shaped quartz tube, a cold trap, and an adsorption trap of molecular sieve; it is directly connected to a gas chromatography-combustion-mass spectrometry (GC-C-MS) system. The sample of ab. 1 g was loaded into the quartz tube and was degassed in helium carrier gas to remove potentially surface-adsorbed gases at 200°C for 4 h. The molecular sieve was activated at 400°C. The CO_2 and hydrocarbon gases were released for 1 h heating at each interval at 3 temperature intervals of 200-400°C, 400-700°C, and 700-1200°C based on volatile releasing patterns in the Pobei complex [10], and were adsorbed and collected using the molecular sieve tube with liquid nitrogen cooling. Then, the CO_2 and hydrocarbon gases were released and introduced into an Agilent 6890 GC-Delta Plus XP-MS system by helium carrier gas for carbon isotope analysis in the Key Lab of Petroleum Resources, CAS, Lanzhou, China. The extraction and analysis methods of volatiles were described in detail by [10, 21, 25]. The reported $\delta^{13}C$ (relative to V-PDB) values have a relative error less than 1.01‰.

3.3.2. He, Ne, and Ar Isotope Analysis. The noble gas isotopes from olivine and pyroxene separates were measured using an online vacuum heating Noblesse mass spectrometer system in the Key Lab of Petroleum Resources, CAS, Lanzhou, China. The sample of about 500 mg was wrapped using aluminum foil and was loaded into the Mo crucible of the sample chamber. The aluminum foil and Mo crucible were preheated for >24 h at 600°C and 1700°C, respectively. The noble gas extraction line and the sample were heated at 150°C for >24 h prior to analysis to remove atmospheric or possibly solar-implanted noble gases adsorbed in the samples.

The volatiles in the sample were extracted by one-step heating at 1200°C. The active gases were removed firstly by using a spongy titanium furnace at 800°C. H_2 was removed by Zr-Al getters at room temperature. The purified noble gases were adsorbed in a cryogenic trap at a temperature of 8 K for 20 min. Then, He, Ne, and Ar gases were released for isotope analysis at the cryogenic trap temperature of 15 K, 50 K, and 100 K, respectively. The volume of He, Ne, and Ar was determined for calibration of their concentration. The air of Lanzhou city collected from the top of Gaolan Mountain in Lanzhou city, China was used as an internal standard, which was measured before each sample. No significant fluctuations were observed during sample analysis. Finally, the measured data were calculated after measuring the voltage ratio of relevant ions from both the standard sample and the sample obtained. The extraction and analysis methods of volatiles are described in detail by [10, 22, 26].

The effect of helium pressure on mass shift was examined and corrected. The mass interferences at $m/z = 22$ of $(^{20}Ne)^+$ and $(^{22}Ne)^+$ from $(^{40}Ar)^{2+}$ and $(^{12}C^{16}O_2)^{2+}$ were corrected using $CO_2{}^{2+}/CO_2{}^{+} = 0.004$. The details of Ne and data correction procedures were described in detail in [22, 26, 27].

4. Results

4.1. The Carbon Isotopic Compositions. The carbon isotopic compositions of CO_2 and CH_4, C_2H_6, C_3H_8, and C_4H_{10} hydrocarbon gases from the olivine (Olv), pyroxene (Pyx), and plagioclase (Pl) separates in the Podong ultramafic intrusion are listed in Table 1.

The Podong magmatic minerals have variable $\delta^{13}C$ values of CO_2 (-24.5‰ to -3.2‰). The $\delta^{13}C_{CO_2}$ range is similar to the Poyi ultramafic intrusion (-33.6–-2.2‰) in the Pobei complex, China [10], the coeval Zhubu ultramafic intrusion (-22.8–-7.1‰) in the Emeishan large igneous province (LIP) [28], and the coeval Noril'sk ultramafic intrusion (-25.3–-19.0‰) in Siberia LIP [20] which were related to mantle plume. $\delta^{13}C_{CO_2}$ values increase from olivine (-24.5–-4.5‰, av. -14.3‰), pyroxene (-22.9–-3.2‰, av. -11.05‰), to plagioclase (-17.2–-6.7‰, av. -11.7‰).

The carbon isotopes of hydrocarbon gases in the Podong intrusion vary in a large range. $\delta^{13}C_{CH_4}$ ranges from -42.6 to -18.4‰, $\delta^{13}C_{C_2H_6} = -34.0$–-18.7‰, $\delta^{13}C_{C_3H_8} = -38.4$–-7.0‰, and $\delta^{13}C_{C_4H_{10}} = -30.9$–-22.5‰. The hydrocarbon gases in most of the samples show normal distribution patterns of carbon isotopes with carbon number (Figure 4(a)), and some samples show (partial) reversal distribution patterns (Figure 4(b)), implying different origins of hydrocarbon gases.

4.2. The He, Ne, and Ar Isotopic Compositions. The He, Ne, and Ar abundances and isotopic compositions of the mineral separates in the Podong ultramafic intrusion are listed in Table 2. $^3He/^4He$ ratios are reported as the R/Ra ratios (i.e., measured $^3He/^4He$ normalized to the atmospheric ratio, $Ra = 1.39 \times 10^{-6}$). The analytical uncertainties for $^3He/^4He$, $^{20}Ne/^{22}Ne$, $^{21}Ne/^{22}Ne$, and $^{40}Ar/^{36}Ar$ ratios are listed as 1σ in Table 2.

The ^4He abundances of olivine and pyroxene minerals in peridotite, pyroxenite, and gabbro in the Podong ultramafic intrusion range from 3.94×10^{-6} cm3 · STP/g to 51.81×10^{-6} cm3 · STP/g, av. 31.61×10^{-6} cm3 · STP/g. The average value of ^4He abundances in pyroxene (30.73×10^{-6} cm3 · STP/g) is lower than that in olivine (av. 37.38×10^{-6} cm3 · STP/g). Podong samples show higher ^4He abundance than the Jinchuan mafic-ultramafic intrusion ($0.01\text{-}2.56 \times 10^{-6}$ cm3 · STP/g) [22] and the Poyi ultramafic intrusion ($0.03\text{-}1.09 \times 10^{-6}$ cm3 · STP/g) [10],

Table 1: The carbon isotopic compositions (‰, V-PDB) of the mineral separates in the Podong mafic-ultramafic intrusion, China.

Sample no.	Rock	Mineral	T (°C)	$\delta^{13}C_{CO_2}$	$\delta^{13}C_{CH_4}$	$\delta^{13}C_{C_2H_6}$	$\delta^{13}C_{C_3H_8}$	$\delta^{13}C_{C_4H_{10}}$
	Olivine	Olv	200-400	-24.5	-26.4			
PD73-2	Gabbro		400-700	-15.7	-31.8	-24.8	-23.2	-29.8
			700-1200	-11.3	-35.5	-23.7	-24.0	-30.9
	Gabbro	Pyx	200-400	-10.5				
PD73-3			400-700	-15.2	-34.7			
			700-1200	-6.3	-38.9			
	Gabbro	Pyx	200-400	-18		-21.1	-20.5	
PD73-4			400-700	-10.6	-20.3			
			700-1200	-5.4	-27.9	-27.9	-38.4	
	Gabbro	Pl	200-400	-17.2	-29.8			
PD73-5			400-700	-11.2	-29.0			
			700-1200	-6.7	-18.9	-26.8	-7.0	
	Gabbro	Pyx	200-400	-20.4	-42.6			
PD73-7			400-700	-10.4	-40.9			
			700-1200	-9.2	-32.4	-24.6	-27.8	-22.5
	Gabbro	Pyx	200-400	-8.5	-31.5			
PD93-3			400-700	-4.3	-22.6			
			700-1200	-6.8	-22.3	-18.7		
	Olivine	Olv	200-400	-22.7	-18.4			
PD93-4	Gabbro		400-700	-7.1	-28.0	-21.4		
			700-1200	-4.5	-27.1	-23.5		
	Olivine	Pyx	200-400	-22.9				
PD93-5	Gabbro		400-700	-20.3	-30.1	-29.7		
			700-1200	-16.0	-30.3	-20.8	-29.8	
	Olivine	Pyx	200-400	-14.8				
PD93-7	Gabbro		400-700	-9.8	-35.8	-34	-28.7	
			700-1200	-10.7	-31.2	-22.5	-25.7	
	Gabbro	Pyx	200-400	-17.9	-40.0			
PD93-8			400-700	-6.1	-36.4	-26.7	-27.9	-24.5
			700-1200	-6.0	-31.5	-24.6		
	Gabbro	Pyx	200-400	-8.4	-26.0	-19.6	-26.3	
PD93-9			400-700	-3.6	-28.3	-23.6	-30.0	
			700-1200	-3.2	-27.2			

Olv: olivine; Pyx: pyroxene; Pl: plagioclase.

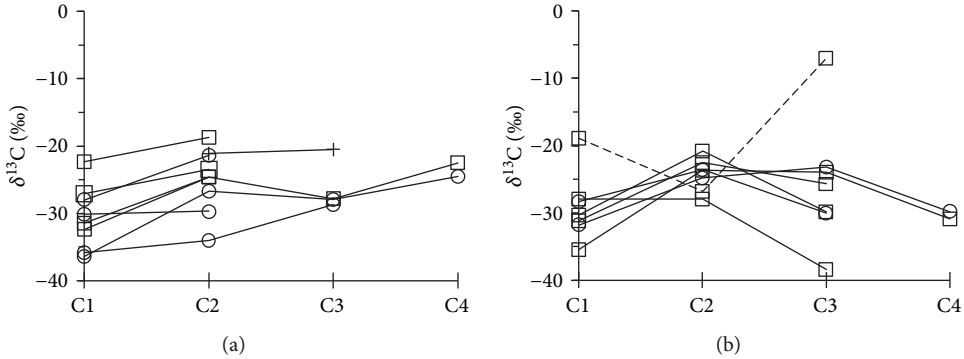

Figure 4: The normal (a) and partial reversal (b) carbon isotopic distribution patterns of CH_4, C_2H_6, C_3H_8, and C_4H_{10} with carbon number in the Podong ultramafic intrusion, China.

Table 2: He, Ne, and Ar abundances and isotopic compositions of the magmatic mineral separates in the Podong mafic-ultramafic intrusion, western China.

No.	Rock	Mineral	Contents (10^{-6} cm3·STP/g)			$^3He/^4He$		$^{20}Ne/^{22}Ne$		$^{21}Ne/^{22}Ne$		$^{40}Ar/^{36}Ar$	
			^4He	^{20}Ne	^{40}Ar	(Ra)	1σ	R	1σ	R	1σ	R	1σ
PD73-1	Pl lherzolite	Pyx	9.49	0.54	41.96	1.16	0.09	9.75	0.23	0.034	0.013	293.05	1.60
PD73-2	Olv gabbro	Olv	33.04	9.55	359.12	0.62	0.03	9.65	0.01	0.029	0.001	297.86	0.50
PD73-4	Gabbro	Pl	27.04	11.50	11.48	1.02	0.04	9.68	0.01	0.029	0.001	126.48	0.52
PD73-5	Gabbro	Pyx	25.06	18.95	682.78	0.90	0.05	9.59	0.21	0.028	0.001	297.19	0.43
PD73-6	Gabbro	Pyx	45.76	3.43	4.15	0.72	0.02	9.75	0.01	0.029	0.002	177.03	7.30
PD73-7	Gabbro	Pyx	29.05	4.60	96.68	1.24	0.03	9.49	0.32	0.028	0.001	295.19	0.78
PD93-1	Pl lherzolite	Pyx	19.75	0.19	22.34	0.41	0.04			0.031	0.001	395.2	1.10
PD93-2	Pl lherzolite	Pyx	3.94	0.17	15.25	1.25	0.15	10.66	0.49	0.032	0.001	398.11	1.50
PD93-3	Gabbro	Pyx	51.81	33.60	68.55	1.10	0.03	9.81	0.01	0.029	0.002	291.92	1.50
PD93-4	Olv gabbro	Olv	41.72	21.26	744.56	1.03	0.04	9.70	0.01	0.029	0.003	294.92	0.40
PD93-7	Olv gabbro	Pyx	50.24	14.40	490.15	1.01	0.04	9.81	0.01	0.028	0.001	301.11	0.52
PD93-6	Gabbro	Pyx	35.07	11.92	451.08	0.84	0.04	9.68	0.01	0.030	0.001	296.23	0.51
PD93-8	Gabbro	Pyx	41.69	1.17	154.42	0.90	0.03			0.023	0.004	296.15	0.73
PD93-9	Gabbro	Pyx	27.83	4.83	185.88	0.98	0.03	9.31	0.51	0.028	0.001	304.69	0.71
PD113-1	Pyroxenite	Pyx	32.70	0.23	18.24	0.29	0.02			0.031	0.001	285.29	9.69

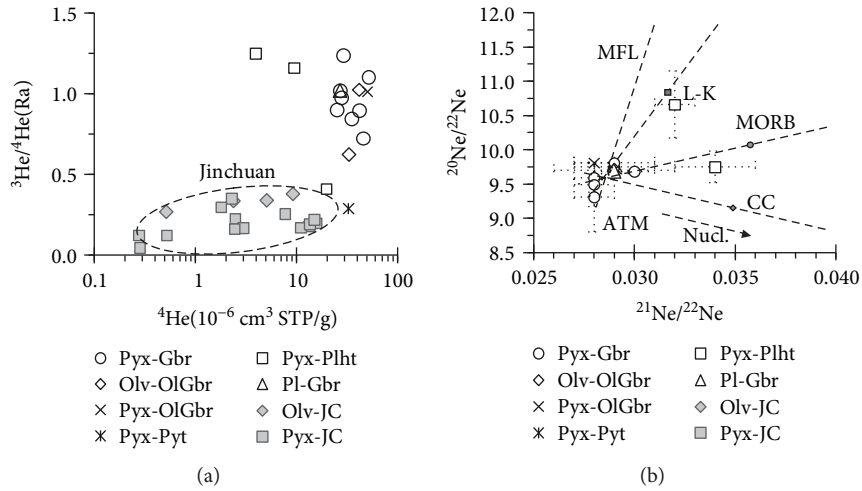

Figure 5: Plots of $^3He/^4He$ versus ^4He contents (a) and $^{20}Ne/^{22}Ne$ versus $^{21}Ne/^{22}Ne$ (b) in the Podong ultramafic intrusion, China. Olv: olivine; Pyx: pyroxene; Gbr: gabbro; OlGbr: olive gabbro; Pyt: pyroxenite; Plht: plagioclase lherzolite; ATM: atmosphere [29, 39]; MFL: the mass fractionation line [29, 39]; CC: continental crust [29]; Nucl.: nucleogenic; L-K: Loihi- Kilauea line [26]; MORB: mid-ocean ridge basalts [58].

China (Figure 5(a)). The Jinchuan mafic-ultramafic intrusion in western China hosts the third largest Ni-Cu sulfide deposit in the world and is of a much older formation age (8.31 Ma) [28] than the Podong intrusion. It should have more radiogenic $^4He^*$ ingrowths produced by U and Th decay after crystallization.

The $^3He/^4He$ ratios of olivine and pyroxene minerals in the Podong ultramafic intrusion range from 0.29 to 1.25 Ra, av. 0.90 Ra. Olivine in the Podong intrusion shows lower $^3He/^4He$ ratios (0.60-1.03 Ra, av. 0.82 Ra) than pyroxene (0.29-1.25 Ra, av. 0.92 Ra). The $^3He/^4He$ ratios of Podong samples are higher than the value of continental crust [29, 30], lower than the values of the subcontinental lithospheric mantle (SCLM, 6.1 Ra) [31–33], arc-related volcanic fluids (5.37 ± 1.87 Ra) [34], typical MORB (8 ± 1 Ra) [35], and OIB (~8-50 Ra) [30, 36, 37]. Podong samples show lower $^3He/^4He$ ratios than the nearby coeval Poyi intrusion (1.13-6.15 Ra) [10] and coeval mafic-ultramafic intrusions in the Emeishan LIP (0.078-4.34 Ra, av. 0.78 Ra) [38] but have higher $^3He/^4He$ ratios than the Jinchuan mafic-ultramafic intrusion, China [22] (Figure 5(a)) with more radiogenic $^4He^*$ ingrowths.

The ^{20}Ne abundances of the Podong intrusion range from 0.17 to 33.60×10^{-6} cm3 · STP/g with a mean of 9.09×10^{-6} cm3 · STP/g. The $^{20}Ne/^{22}Ne$ ratios in the

Podong intrusion vary from 9.31 to 10.66, and the $^{21}Ne/^{22}Ne$ ratios range from 0.027 to 0.035 (Figure 5(b)). The $^{20}Ne/^{22}Ne$ ratios are lower than the mantle (12.5), higher than the atmospheric value (9.8) [29, 39, 40]. The $^{21}Ne/^{22}Ne$ ratios are within the ranges of the atmosphere (0.029) and the solar value (0.033) and are lower than the crust (0.47) and the upper mantle (0.074) [39–43]. $^{20}Ne/^{22}Ne$ and $^{21}Ne/^{22}Ne$ are plotted around Air and show a trend to the L-K line (Figure 5(b)).

The ^{40}Ar abundances of the Podong intrusion range from 4.15 to 744.56×10^{-6} cm3 · STP/g, which is much higher than the Jinchuan intrusion (0.04-21.70×10^{-6} cm3 · STP/g) [22] and the Poyi intrusion (0.14-0.50×10^{-6} cm3 · STP/g) [10]. The $^{40}Ar/^{36}Ar$ ratios in the Podong intrusion vary from 285.29 to 398.11, which are close to the atmosphere (295.5) and lower than the crust (1650–170000) and the mantle (295.5-8000) [36, 42, 44–46].

5. Discussion

5.1. The Origins of Magmatic Volatiles. The volatiles had occurred in the Poyi and Podong intrusions (Figure 3) and had played a key role in the processes of triggering sulfide saturation and mineralization [3, 4, 10, 11]. The CO_2 and CH_4 volatiles and noble gases released from the Podong samples could be derived from three potential sources: (1) primary volatiles in the Podong magmatism, including mantle-derived volatiles from partial melting of mantle source and contaminated crustal volatiles from subducted plate or country rocks, (2) *in situ* radiogenic noble gas ingrowths produced by U, Th, and K decay after mineral crystallization, and (3) secondary volatiles added by subsequent alteration or regional metamorphism and contaminated air and cosmogenic noble gases. The third source of volatiles absorbed on sample surface is likely negligible in the Podong samples due to fresh core samples with less alteration or metamorphism, as well as sample pretreatment before analysis [22, 41, 47]. Therefore, volatiles released from the Podong samples could be derived from magmatism and radiogenic noble gas ingrowths and can trace the origins of the volatiles.

The volatiles of different origins exhibit markedly different C, He, Ne, and Ar isotopic compositions, which can be used to reveal their sources [10, 21, 22, 28, 37, 48]. The $^{3}He/^{4}He$ and $^{40}Ar/^{36}Ar$ ratios in the Podong intrusion are mainly plotted around the atmosphere (ATM) with a trend toward continental crust and old oceanic crust end-members [22, 29, 39, 49] (crust, Figure 6). The $^{20}Ne/^{22}Ne$ and $^{21}Ne/^{22}Ne$ ratios of most Podong samples were also plotted around the ATM and show a trend to the L-K line and MORB (i.e., upper mantle, DMM) (Figure 5(b)) [27, 29, 50].

Low $^{3}He/^{4}He$ ratios of Podong samples could be interpreted as *in situ* radiogenic ^{4}He ingrowths, crust and air-saturated fluid additions (Figures 5(a) and 6), because mantle-derived He signatures are often diluted by the addition of *in situ* radiogenic ^{4}He [43] and/or crustal He [29, 30]. The radiogenic ingrowths produced by U, Th, and K decay after crystallization can be deduced by calculation

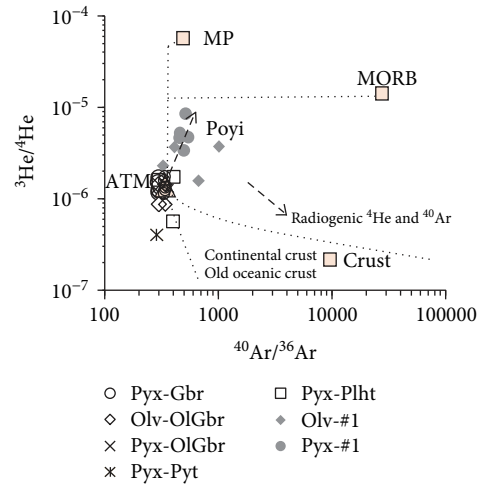

FIGURE 6: Plot of $^{40}Ar/^{36}Ar$ versus $^{3}He/^{4}He$ ratios in the Podong intrusion, China (after [49]). ATM: atmosphere [29, 39]; Crust: continental crust; MORB: depleted mantle for MORB; MP: mantle plume [34, 35]. Data sources: the Poyi ultramafic intrusion, China (#1) [10].

or be identified by the relationship between isotopic ratios and contents of He and Ar.

The amounts of radiogenic $^{4}He^{*}$ contents in the Podong intrusion can be calculated using Graham et al.'s (1987) equation:

$$^{4}He^{*} = 2.80 \times 10^{-8}(4.35 + Th/U)[U] \cdot t(cm3 \cdot STP/g), \quad (1)$$

where t is the formation time in Myr, [U] is the uranium concentration in ppm, and Th/U is the atomic ratio of Th and U. Using average contents of whole rock Th (0.15, 0.24, and 0.11 ppm) and U (0.04, 0.08, and 0.06 ppm) for lherzolite, pyroxenite, and gabbro, respectively [3, 4], and the crystallization age of the gabbro (270 Ma) in the Podong intrusion [4], the estimated radiogenic $^{4}He^{*}$ contents are 2.45, 4.45, and 2.80×10^{-6} cm3 · STP/g for lherzolite, pyroxenite and gabbro, respectively.

The whole rock K contents (0.07, 0.08, and 0.14 wt%) for lherzolite, pyroxenite and gabbro [3, 4] were used to estimate the radiogenic $^{40}Ar^{*}$ contents as 0.11, 0.13 and 0.22×10^{-6} cm3·STP/g in lherzolite, Pyroxenite and Gabbro, respectively.

The estimated radiogenic $^{4}He^{*}$ and $^{40}Ar^{*}$ contents in the Podong ultramafic intrusion range from 2.45 to 4.45×10^{-6} cm3 · STP/g and from 0.11 to 0.23×10^{-6} cm3 · STP/g, respectively, and are much lower than the measured values (Table 2). There is no obvious correlation between $^{3}He/^{4}He$ and ^{4}He contents, which can rule out significant radiogenic $^{4}He^{*}$ ingrowths in the Podong samples (Figure 5(a)). The obvious correlation between $^{40}Ar/^{36}Ar$ ratios and ^{40}Ar contents indicated a certain amount of radiogenic $^{40}Ar^{*}$ ingrowths (Figures 7(a) and 7(b)). $^{3}He/^{4}He$ and $^{40}Ar/^{36}Ar$ ratios after deducting radiogenic $^{4}He^{*}$ and $^{40}Ar^{*}$ contents show similar ranges to measured values and indicate a large proportion of air and crust origins (Figure 6).

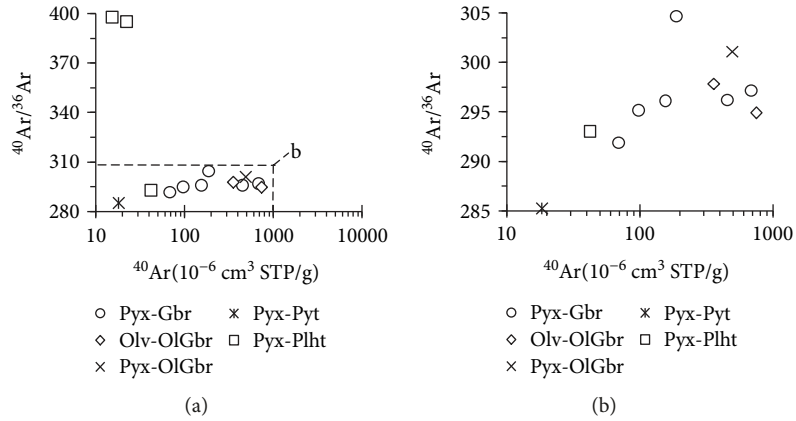

Figure 7: Plots of $^{40}Ar/^{36}Ar$ versus ^{40}Ar contents (a) and partial enlarged (b) in the Podong intrusion, China.

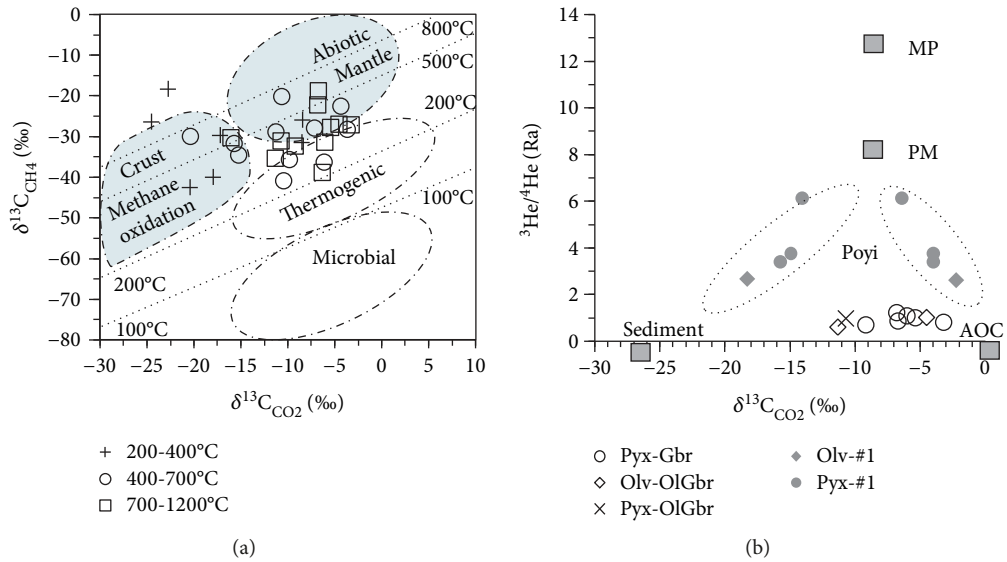

Figure 8: The plots of $\delta^{13}C_{CO_2}$ (‰, v-PDB) vs. $\delta^{13}C_{CH_4}$ (‰, v-PDB) (a, [52]) and the $^3He/^4He$ ratios (b, [10]) in the Podong ultramafic intrusion, China. Thermogenic: thermogenic origins [52]; Sediment: sedimentary organic matter [63]; AOC: altered oceanic crust [64]; MP: mantle plume [34]; PM: primitive mantle [34, 40].

The CO_2 and hydrocarbon gases from different origins show distinct carbon isotopic compositions and distribution patterns, which can be used to constrain various terrestrial reservoirs [10, 21, 22, 37, 48, 51]. The CO_2 and CH_4 released at 200-400°C were mainly released from secondary fluid inclusions and cracked primary fluid inclusions (Figure 3(b)), since the atmospheric component adsorbed in the samples is generally degassed at low temperature during step heating [49]. $\delta^{13}C_{CO_2}$ and $\delta^{13}C_{CH_4}$ values at 200-400°C are plotted into the range associated with methane oxidation and crustal origins (Figure 8(a)) and proved the origin of secondary processes, i.e., alteration.

The CO_2 and hydrocarbon gases released at 400-700°C and 700-1200°C temperature intervals from the Podong samples were mainly released from the fluid inclusions trapped during the magmatic process (Figure 3(a)). $\delta^{13}C_{CO_2}$ and $\delta^{13}C_{CH_4}$ are plotted into the ranges of the mantle, thermogenic, and crust-methane oxidation origins (Figure 8(a)) [10, 49, 52], indicating that the Podong volatiles originated from the mantle (i.e., abiogenic origin) [53, 54] and were mixed with thermogenic and crustal components. The mantle origin of volatiles is supported by (partial) reversal carbon isotopic distribution pattern of the hydrocarbon gases (Figure 4(b)), i.e., abiogenic hydrocarbon gases. It is also supported by sulfur isotopes of sulfide separates (0.82-2.02‰) [3], similar to typical mantle values (0 ± 2‰). The thermogenic origin refers to the gases formed by thermal decomposition of biogenic organic matter under high geological temperature and pressure conditions and implies a sedimentary source [48]. The crust and thermogenic origins are supported by a normal carbon isotopic distribution pattern (Figure 4(a)).

The C, He, and Ar isotopes depict a mixture of different end-members for the Podong mafic-ultramafic rocks. The proportions of each end-member can be estimated by mass balance calculations of He and Ar isotopic mixing models. The air-saturated fluid (ASF) has low $^{3}He/^{4}He$ (1 Ra) and $^{40}Ar/^{36}Ar$ (298.6) [29, 55]; recycled oceanic crust has low $^{3}He/^{4}He$ (0.005 Ra) [30] and $^{40}Ar/^{36}Ar$ (350) [56]. The upper mantle (UM) or subcontinental lithospheric mantle (SCLM) has high $^{3}He/^{4}He$ (6.1 Ra) [31–33] and $^{40}Ar/^{36}Ar$ (2000) ratios [31]. The SCLM and crust are considered as the only two end-members of the He isotopic mixing model to calculate the proportions of SCLM and crust components due to very low He concentration and the shortest atmospheric residence time (1 to 10 million years) in the atmosphere [22]. Calculation shows 5-26%, av. 18% for SCLM, av. 10% for altered oceanic crust, and av. 72% for ASF, i.e., ATM, when radiogenic $^{4}He^{*}$ has been corrected from silicate mineral separates. The most ATM component could be volatiles from ASF.

5.2. The Additions of Air and Crustal Volatiles. The carbon and noble gas isotopic compositions indicated that a large proportion of air and crustal components had been mixed in the Podong mantle-derived magma (Figures 4(b) and 5(a)). The low $^{3}He/^{4}He$ ratios and calculated contents of radiogenic $^{4}He^{*}$ imply a large proportion of crustal origin in the Podong intrusion, which was supported by pronounced negative Nb-Ta anomalies and whole-rock Sr-Nd isotopes [4]. Large proportions of air are suggested by low $^{40}Ar/^{36}Ar$ and $^{21}Ne/^{22}Ne$ ratios in the Podong samples.

The type of assimilated crustal materials in the Podong intrusion was inferred as siliceous materials of the upper crust, pre-Permian sedimentary rocks in region [3], or crustal fluid [4]. The crust siliceous materials contaminated in the Podong magma can not only result in low $^{3}He/^{4}He$ ratios but also cause the rising of both $^{40}Ar/^{36}Ar$ and $^{21}Ne/^{22}Ne$ ratios. Meanwhile, a large proportion of siliceous materials (at least 0–13 wt% [3]) should cause a significant increase in the SiO_2 content of the magma system, i.e., more felsic rocks. All of those are not observed in the Podong intrusion (Figure 6). Therefore, large proportions of contaminated crust materials could be fluids, but siliceous materials, as shown above in the calculations of He and Ar isotopic mixing models.

The siliceous and fluids are two types of crustal materials that could exist in the Podong magma. Xue et al. argued that 0–13 wt% crustal contamination suggested by Sr-Nd isotopes in the Podong parental magma cannot fully account for the observed negative Nb-Ta anomalies in the rocks [3], which implied more crustal materials related to negative Nb-Ta anomalies. The fluids associated with the subducted plate could be the best candidate without siliceous materials.

The $\delta^{13}C_{CO_2}$ vs. $\delta^{13}C_{CH_4}$ plotted the Podong samples into ranges of thermogenic, crust-methane oxidation, and mantle (Figure 8(a)). The normal $\delta^{13}C$ distribution pattern from CH_4 to C_4H_{10} observed in most Podong samples suggests that hydrocarbon gases should be biogenic organic matters, i.e., contaminated crustal components in Podong magma could derive from sedimentary organic matters (Figure 4(a)), including sedimentary organic matters from country rocks of magma chamber or/and subducted plate in the magma source. The $\delta^{13}C_{CO_2}$ values increase from olivine, pyroxene, to plagioclase and constrain that crustal materials with heavy $\delta^{13}C$ were added into magma during crystallization in the magma chamber. Therefore, assimilation of crustal material should occur during crystallizing in the magma chamber.

A large proportion of atmosphere component in the Podong intrusion is suggested by Ne and Ar isotopes (Figures 5(b) and 7(b)). $^{20}Ne/^{22}Ne$ and $^{21}Ne/^{22}Ne$ ratios in the Podong intrusion are mainly plotted around ATM (Figure 5(b)); $^{40}Ar/^{36}Ar$ vs. $^{3}He/^{4}He$ diagram also indicated a large proportion of air in the Podong magma (Figures 5(a), 7(a), and 7(b)). The $^{40}Ar/^{36}Ar$ and $^{21}Ne/^{22}Ne$ ratios in the Podong intrusion are very low and could be related to the incorporation of atmospheric components [57] or recycled oceanic crust in the source materials [58], although the radiogenic $^{40}Ar^{*}$ ingrowths were suggested by calculation and the relationship of $^{40}Ar/^{36}Ar$ versus ^{40}Ar content (Figure 7(a)). The $\delta^{13}C_{CO_2}$ and $^{3}He/^{4}He$ ratios of the Podong ultramafic intrusion plotted a trend of the altered oceanic crust (AOC, Figure 8(b)), so a large proportion of atmosphere component could be related to the ASF devolatilization of recycled oceanic crust in the magma source.

5.3. The Petrogenesis and Dynamic Settings of Intrusion. Carbon and noble gas isotopes indicate that the Podong intrusion could have a different petrogenesis from the Poyi ultramafic intrusion (Figures 6 and 8(b)). C-He-Ar and Sr-Nd isotopes indicate that the Podong and Poyi ultramafic intrusions did not share the same mantle source [3]. It is supported by the significant difference of Sr-Nd isotope compositions between the Podong and Poyi coeval mafic-ultramafic intrusions [3]. The Podong intrusion shows lower calculated $\varepsilon Nd(t)$ values and higher initial $(^{87}Sr/^{86}Sr)_i$ ratios than the coeval Poyi mafic-ultramafic intrusion (see Figure 10a in reference [3]). The Podong ultramafic intrusion could have a magma source of lithospheric mantle, which was metasomatized by slab-derived fluids and/or subducted sediment-derived melt during the previous subduction processes [3]. The Podong magma should be formed by the partial melting of metasomatized lithospheric mantle material with higher $(^{87}Sr/^{86}Sr)_i$ and lower $\varepsilon Nd(t)$ than Poyi intrusion and was contaminated by the crustal components in the magma chamber.

The $\delta^{13}C_{CO_2}$, $^{3}He/^{4}He$, and $^{40}Ar/^{36}Ar$ ratios of the Podong ultramafic intrusion are plotted around the air (ATM) with a trend to the altered oceanic crust (AOC, Figures 6 and 8(b)) and are different from the Poyi ultramafic intrusion. The Poyi intrusion showed a trend to mantle plume with high $^{3}He/^{4}He$ and $^{40}Ar/^{36}Ar$ ratios [10] (Figure 8(b)). Mantle plume has a $^{3}He/^{4}He$ value of ~12.7 Ra [36] and $^{40}Ar^{36}Ar$ of 1200 [50]. The high $^{3}He/^{4}He$ ratios of 8-50 Ra observed in many mantle

plumes are from an ancient reservoir created within the first 100 Myr of solar system histories [36, 59, 60]. The noble gas isotopes had not completely homogenized in the mantle due to low recycling efficiency in the mantle compared to the lithophile elements [59]. The primordial noble gases that supply mantle plumes are not distributed throughout the whole lower mantle or are localized in a region of the deep mantle [59]. The mantle plume existing beneath the Poyi intrusion could provide less contribution of real materials (e.g., of silicate and fluid components) in the Podong magma because the associated Podong mafic dykes show similar Sr-Nd isotope ranges to the coeval Poyi mafic-ultramafic intrusion [3], i.e., Podong magmatism could be a little older (270 ± 2.7 Ma [3] or 273.5 ± 2.9 Ma [4]) than the Poyi magma (269.9 ± 1.7 Ma [2]) associated mantle plume.

The ATM and crustal components added in the Podong magma could be derived from either subducted sedimentary organic matter in the mantle source or contaminations from country rocks in magma chambers or rising conduit. The subduction of the oceanic crust can effectively transport air and crust components into the mantle [7, 40, 50] because the recycled oceanic crust has low He contents, extremely low $^{3}He/^{4}He$ (<0.1 Ra) [61], and relatively low $^{40}Ar/^{36}Ar$ (350) [46]; meanwhile, subducted oceanic crust has variable $\delta^{13}C_{CO_2}$ values ranging from -26‰ for type I organic-rich sediments of altered ocean crust (AOC) to 0‰ for marine carbonate [10, 62, 63].

The correlations between $^{3}He/^{4}He$ ratio vs. both $^{40}Ar/^{36}Ar$ and $\delta^{13}C_{CO_2}$ indicated the contribution from altered oceanic crust (AOC, Figures 6 and 8) in the Podong intrusion [64, 65]. $\delta^{13}C_2 > \delta^{13}C_3$ in most samples demonstrate type I organic materials from oceanic sedimentary [48]. The $\delta^{13}C_{CO_2}$ and $\delta^{13}C_{CH_4}$ variations in the Podong volatiles are suggestive of methane oxidative activity (Figure 8(a)), which provides further evidence of a contribution from altered oceanic crust [10]. All the evidences make the subducted altered ocean crust (AOC) as probable end-member to explain the C-He-Ne-Ar isotopic compositions of the Podong samples (Figure 8(b)). This is consistent with a subduction-modified mantle source suggested by LILE rich and Nb and Ta depletion [4, 13] because subduction-related magma is commonly characterized by pronounced negative Nb-Ta anomalies.

The noble gases are stored in sedimentary organic matter with air-saturated fluid (ASF) and are highly soluble in hydrous minerals such as amphibole and phlogopite [44]. The fluid-related components from the altered oceanic crust with low K, U, and Th contents could be the favorite candidate for added air and crustal components, which were supported by contributions from water or other volatile phases in the Podong intrusion [3, 4]. The water and other fluids in the parental magma were indicated by common occurrence of hornblende and phlogopite in the intrusion (Figure 3(c)) [3]. Enhanced recycling of subducted altered oceanic components to the mantle source region can account for the relatively low ratios of He, Ne, and Ar isotopes.

6. Conclusions

The C and He-Ne-Ar isotopic data of the Podong ultramafic intrusion provide the evidence for air and crustal origins as well as petrogenesis.

(1) Most of the Podong magmatic minerals show normal carbon isotopic distribution patterns of CH_4, C_2H_6, C_3H_8, and C_4H_{10} that indicated hydrocarbon gases of sedimentary origin. The variable $\delta^{13}C_{CO_2}$ and light $\delta^{13}C_{CH_4}$ suggested that the mantle-derived magmatic volatiles were mixed with thermogenic and crustal components

(2) Low $^{3}He/^{4}He$, $^{21}Ne/^{22}Ne$, and $^{40}Ar/^{36}Ar$ ratios indicated a large proportion of air and crustal components mixed in the Podong intrusion. Two types of contaminated crustal materials can be identified as crustal fluids from the altered oceanic crust and siliceous crust materials. The crustal materials of country rock were assimilated during magma crystallizing in the chamber

(3) Carbon and noble gas isotopes indicated that the Podong intrusion could have a different petrogenesis from the nearby coeval Poyi ultramafic intrusion. Subducted oceanic plate added air and crustal fluids released from altered oceanic crust with a large proportion of ASF into the magma SCLM source. The mantle plume beneath the Poyi intrusion could contribute less real material of silicate and fluid components

Data Availability

The manuscript is a self-contained data article; the entire data used to support the findings of this study are included within the article. If any additional information is required, this is available from the corresponding author upon request to mjzhang@lzu.edu.cn.

Additional Points

Highlight. The Podong ultramafic intrusion hosts the only massif Ni-Cu sulfide mineralization in the Pobei layered mafic-ultramafic complex, China, and had different petrogenesis with fewer mantle plume contributions from the nearby coeval the Poyi intrusion related mantle plume (Zhang et al., Chem. Geol., 2017).

Conflicts of Interest

The authors declare that there are no conflicts of interest regarding the publication of this paper.

Acknowledgments

This study was financially supported by NSF of China (41872075, 41572136, 41502143, 41473062, and 41372095),

STEP program (Grant no. 2019QZKK0704), Gansu Key Lab of Petrol. Res. (SZDKFJJ20170603), and DPHEC (20120211110023). We thank Gang Deng, Jiangwei Zhang, Zhaowei Zhang, Qingyan Tang, Jianping Li, Zhe Song, Chunhui Cao and Li Du for their assistance in fieldwork, sampling, and experimental works.

References

[1] K. Qin, B. Su, P. A. Sakyi et al., "SIMS zircon U-Pb geochronology and Sr-Nd isotopes of Ni-Cu-Bearing Mafic-Ultramafic Intrusions in Eastern Tianshan and Beishan in correlation with flood basalts in Tarim Basin (NW China): Constraints on a *ca*. 280 Ma mantle plume," *American Journal of Science*, vol. 311, no. 3, pp. 237–260, 2011.

[2] S. C. Xue, C. Li, K. Z. Qin, and D. M. Tang, "A non-plume model for the Permian protracted (266–286 Ma) basaltic magmatism in the Beishan–Tianshan region, Xinjiang, Western China," *Lithos*, vol. 256-257, pp. 243–249, 2016.

[3] S. Xue, K. Qin, C. Li, Z. Yao, E. M. Ripley, and X. Wang, "Geochronological, mineralogical and geochemical studies of sulfide mineralization in the Podong mafic-ultramafic intrusion in northern Xinjiang, western China," *Ore Geology Reviews*, vol. 101, pp. 688–699, 2018.

[4] J. Jiao, X. Leng, S. Duan, M. Xia, H. Rui, and L. Tan, "Petrogenesis and metallogenic characteristics of the Early Permian Podong Cu-Ni sulfide deposit, northeastern margin of the Tarim plate," *Acta Petrologica Sinica*, vol. 34, no. 8, pp. 2211–2222, 2018.

[5] S. H. Yang, M. F. Zhou, P. C. Lightfoot et al., "Re–Os isotope and platinum-group element geochemistry of the Pobei Ni–Cu sulfide-bearing mafic–ultramafic complex in the northeastern part of the Tarim Craton," *Mineralium Deposita*, vol. 49, no. 3, pp. 381–397, 2014.

[6] B. Su, K. Qin, P. A. Sakyi et al., "Geochronologic-petrochemical studies of the Hongshishan mafic–ultramafic intrusion, Beishan area, Xinjiang (NW China): petrogenesis and tectonic implications," *International Geology Review*, vol. 54, no. 3, pp. 270–289, 2012.

[7] Q. Tang, M. Zhang, W. Li, M. Yu, Z. Zhang, and Y. Wang, "Geodynamic setting and metallogenic potential of Permian large-sized mafic-ultramafic intrusions in Beishan area, Xinjiang, China," *Geology in China*, vol. 42, no. 3, pp. 468–481, 2015.

[8] Y. Liu, X. Lu, C. Wu et al., "The migration of Tarim plume magma toward the northeast in Early Permian and its significance for the exploration of PGE-Cu–Ni magmatic sulfide deposits in Xinjiang, NW China: As suggested by Sr–Nd–Hf isotopes, sedimentology and geophysical data," *Ore Geology Reviews*, vol. 72, pp. 538–545, 2016.

[9] J. Ma, X. Lu, Y. Liu et al., "The impact of early sulfur saturation and calc-crustal contamination on ore-forming process in the Posan mafic–ultramafic complex: derived from the shallow depleted mantle, Beishan region, NW China," *Journal of Asian Earth Sciences*, vol. 118, pp. 81–94, 2016.

[10] M. Zhang, Q. Tang, C. Cao et al., "The origin of Permian Pobei ultramafic complex in the northeastern Tarim craton, western China: evidences from chemical and C-He-Ne-Ar isotopic compositions of volatiles," *Chemical Geology*, vol. 469, pp. 85–96, 2017.

[11] P. Feng, M. Zhang, L. Li et al., "The noble gas isotopic constrains on the petrogenesis of mafic-ultramafic intrusions in the western end of the Pobei complex, Xinjiang, northwestern China," *Acta Petrologica Sinica*, vol. 34, no. 11, pp. 3445–3454, 2018.

[12] X. Y. Song, L. M. Chen, Y. F. Deng, and W. Xie, "Syncollisional tholeiitic magmatism induced by asthenosphere upwelling owing to slab detachment at the southern margin of the Central Asian Orogenic Belt," *Journal of the Geological Society*, vol. 170, no. 6, pp. 941–950, 2013.

[13] M. Z. Xia, C. Y. Jiang, C. Li, and Z. D. Xia, "Characteristics of a newly discovered Ni-Cu sulfide deposit hosted in the Poyi ultramafic intrusion, Tarim Craton, NW China," *Economic Geology*, vol. 108, no. 8, pp. 1865–1878, 2013.

[14] S. Xue, K. Qin, C. Li et al., "Geochronological, petrological and geochemical constraints on Ni-Cu sulfide mineralization in the Poyi ultramafic-troctolitic intrusion in the northeast rim of the Tarim Craton, western China," *Economic Geology*, vol. 111, no. 6, pp. 1465–1484, 2016.

[15] B. Su, K. Qin, H. Sun, and H. Wang, "Geochronological, petrological, mineralogical and geochemical studies of the Xuanwoling mafic-ultramafic intrusion in Beishan area, Xinjiang," *Acta Petrologica Sinica*, vol. 26, no. 11, pp. 3283–3294, 2010.

[16] B. X. Su, K. Z. Qin, M. Santosh, H. Sun, and D. M. Tang, "The Early Permian mafic–ultramafic complexes in the Beishan Terrane, NW China: Alaskan-type intrusives or rift cumulates?," *Journal of Asian Earth Sciences*, vol. 66, pp. 175–187, 2013.

[17] S. J. Ao, W. J. Xiao, C. M. Han, Q. G. Mao, and J. E. Zhang, "Geochronology and geochemistry of early Permian mafic–ultramafic complexes in the Beishan area, Xinjiang, NW China: implications for late paleozoic tectonic evolution of the southern Altaids," *Gondwana Research*, vol. 18, no. 2-3, pp. 466–478, 2010.

[18] H. Wang, P. Wang, J. Li, J. Feng, G. Deng, and X. Lv, "A tentative discussion on features of mafic-ultramafic rocks and exploration methods in Pobei area of Ruoqiang, Xinjiang," *Geology in China*, vol. 42, no. 3, pp. 777–784, 2015.

[19] M. Moreira and P. Madureira, "Cosmogenic helium and neon in 11 Myr old ultramafic xenoliths: Consequences for mantle signatures in old samples," *Geochemistry, Geophysics, Geosystems*, vol. 6, no. 8, article Q08006, 2005.

[20] Q. Tang, M. Zhang, C. Li, M. Yu, and L. Li, "The chemical compositions and abundances of volatiles in the Siberian large igneous province: constraints on magmatic CO_2 and SO_2 emissions into the atmosphere," *Chemical Geology*, vol. 339, pp. 84–91, 2013.

[21] M. Zhang, P. Hu, Y. Niu, and S. Su, "Chemical and stable isotopic constraints on the nature and origin of volatiles in the sub-continental lithospheric mantle beneath eastern China," *Lithos*, vol. 96, no. 1-2, pp. 55–66, 2007.

[22] M. Zhang, Q. Tang, P. Hu, X. Ye, and Y. Cong, "Noble gas isotopic constraints on the origin and evolution of the Jinchuan Ni-Cu-(PGE) sulfide ore-bearing ultramafic intrusion, Western China," *Chemical Geology*, vol. 339, pp. 301–312, 2013.

[23] M. F. Miller and C. T. Pillinger, "An appraisal of stepped heating release of fluid inclusion CO^2 for isotopic analysis: A preliminary to $\delta^{13}C$ characterisation of carbonaceous vesicles at the nanomole level," *Geochimica et Cosmochimica Acta*, vol. 61, no. 1, pp. 193–205, 1997.

[24] P. H. Barry, D. R. Hilton, E. Füri, S. A. Halldórsson, and K. Grönvold, "Carbon isotope and abundance systematics of

Icelandic geothermal gases, fluids and subglacial basalts with implications for mantle plume-related CO_2 fluxes," *Geochimica et Cosmochimica Acta*, vol. 134, pp. 74–99, 2014.

[25] Z. Li, X. Wang, L. Li et al., "Development of new method of $\delta^{13}C$ measurement for trace hydrocarbons in natural gas using solid phase micro-extraction coupled to gas chromatography isotope ratio mass spectrometry," *Journal of Chromatography A*, vol. 1372, pp. 228–235, 2014.

[26] C. Cao, M. Zhang, Q. Tang et al., "Noble gas isotopic variations and geological implication of Longmaxi shale gas in Sichuan Basin, China," *Marine and Petroleum Geology*, vol. 89, pp. 38–46, 2018.

[27] T. Zhang, M. Zhang, B. Bai, X. Wang, and L. Li, "Origin and accumulation of carbon dioxide in the Huanghua depression, Bohai Bay basin, China," *AAPG Bulletin*, vol. 92, no. 3, pp. 341–358, 2008.

[28] M. Zhang, S. L. Kamo, C. Li, P. Hu, and E. M. Ripley, "Precise U–Pb zircon–baddeleyite age of the Jinchuan sulfide ore-bearing ultramafic intrusion, western China," *Mineralium Deposita*, vol. 45, no. 1, pp. 3–9, 2010.

[29] C. J. Allègre, T. Staudacher, and P. Sarda, "Rare gas systematics: formation of the atmosphere, evolution and structure of the Earth's mantle," *Earth and Planetary Science Letters*, vol. 81, no. 2-3, pp. 127–150, 1987.

[30] C. J. Ballentine and P. G. Burnard, "Production, release and transport of noble gases in the continental crust," *Reviews in Mineralogy and Geochemistry*, vol. 47, no. 1, pp. 481–538, 2002.

[31] T. J. Dunai and H. Baur, "Helium, neon, and argon systematics of the European subcontinental mantle: Implications for its geochemical evolution," *Geochimica et Cosmochimica Acta*, vol. 59, no. 13, pp. 2767–2783, 1995.

[32] C. Gautheron and M. Moreira, "Helium signature of the subcontinental lithospheric mantle," *Earth and Planetary Science Letters*, vol. 199, no. 1-2, pp. 39–47, 2002.

[33] C. Gautheron, M. Moreira, and C. Allègre, "He, Ne and Ar composition of the European lithospheric mantle," *Chemical Geology*, vol. 217, no. 1-2, pp. 97–112, 2005.

[34] D. R. Hilton, T. P. Fischer, and B. Marty, "Noble gases and volatile recycling at subduction zones," *Reviews in Mineralogy and Geochemistry*, vol. 47, no. 1, pp. 319–370, 2002.

[35] K. A. Farley, J. H. Natland, and H. Craig, "Binary mixing of enriched and undegassed (primitive?) mantle components (He, Sr, Nd, Pb) in Samoan lavas," *Earth and Planetary Science Letters*, vol. 111, no. 1, pp. 183–199, 1992.

[36] A. R. Basu, R. J. Poreda, P. R. Renne et al., "High-^{3}He plume origin and temporal-spatial evolution of the Siberian flood basalts," *Science*, vol. 269, no. 5225, pp. 822–825, 1995.

[37] D. R. Hilton and D. Porcelli, "3.7 - Noble gases as mantle tracers," in *Treatise on Geochemistry (Second Edition)*, vol. 3, pp. 293–325, 2014.

[38] T. Hou, Z. Zhang, X. Ye, J. Encarnacion, and M. K. Reichow, "Noble gas isotopic systematics of Fe–Ti–V oxide ore-related mafic–ultramafic layered intrusions in the Panxi area, China: the role of recycled oceanic crust in their petrogenesis," *Geochimica et Cosmochimica Acta*, vol. 75, no. 22, pp. 6727–6741, 2011.

[39] P. Sarda, T. Staudacher, and C. Allegre, "Neon isotopes in submarine basalts," *Earth and Planetary Science Letters*, vol. 91, no. 1-2, pp. 73–88, 1988.

[40] P. Sarda, M. Moreira, T. Staudacher, J. G. Schilling, and C. J. Allegre, "Rare gas systematics on the southernmost Mid-Atlantic Ridge: constraints on the lower mantle and the Dupal source," *Journal of Geophysical Research*, vol. 105, no. B3, pp. 5973–5996, 2000.

[41] J. P. Benkert, H. Baur, P. Signer, and R. Wieler, "He, Ne, and Ar from the solar wind and solar energetic particles in lunar ilmenites and pyroxenes," *Journal of Geophysical Research*, vol. 98, no. E7, pp. 13147–13162, 1993.

[42] R. K. O'Nions and I. N. Tolstikhin, "Behaviour and residence times of lithophile and rare gas tracers in the upper mantle," *Earth and Planetary Science Letters*, vol. 124, no. 1-4, pp. 131–138, 1994.

[43] M. Ozima and F. A. Podosek, *Noble Gas Geochemistry*, Cambridge University Press, Cambridge, UK, 2nd edition, 2002.

[44] M. A. Kendrick, M. Honda, D. Gillen, T. Baker, and D. Phillips, "New constraints on regional brecciation in the Wernecke Mountains, Canada, from He, Ne, Ar, Kr, Xe, Cl, Br and I in fluid inclusions," *Chemical Geology*, vol. 255, no. 1–2, pp. 33–46, 2008.

[45] M. Moreira, J. Kunz, and C. Allegre, "Rare gas systematics in popping rock: isotopic and elemental compositions in the upper mantle," *Science*, vol. 279, no. 5354, pp. 1178–1181, 1998.

[46] T. Staudacher, P. Sarda, S. H. Richardson, C. J. Allègre, I. Sagna, and L. V. Dmitriev, "Noble gases in basalt glasses from a Mid-Atlantic Ridge topographic high at 14°N: geodynamic consequences," *Earth and Planetary Science Letters*, vol. 96, no. 1-2, pp. 119–133, 1989.

[47] D. Lal, "In situ-produced cosmogenic isotopes in terrestrial rocks," *Annual Review of Earth and Planetary Sciences*, vol. 16, no. 1, pp. 355–388, 1988.

[48] M. Zhang, Q. Tang, C. Cao et al., "Molecular and carbon isotopic variation in 3.5 years shale gas production from Longmaxi Formation in Sichuan Basin, China," *Marine and Petroleum Geology*, vol. 89, pp. 27–37, 2018.

[49] M. Moreira and P. Sarda, "Noble gas constraints on degassing processes," *Earth and Planetary Science Letters*, vol. 176, no. 3-4, pp. 375–386, 2000.

[50] D. W. Graham, "Noble gas isotope geochemistry of mid-ocean ridge and ocean island basalts: characterization of mantle source reservoirs," *Reviews in Mineralogy and Geochemistry*, vol. 47, no. 1, pp. 247–317, 2002.

[51] Q. Tang, M. Zhang, Y. Wang et al., "The origin of the Zhubu mafic-ultramafic intrusion of the Emeishan large igneous province, SW China: Insights from volatile compositions and C-Hf-Sr-Nd isotopes," *Chemical Geology*, vol. 469, pp. 47–59, 2017.

[52] Y. Ueno, K. Yamada, N. Yoshida, S. Maruyama, and Y. Isozaki, "Evidence from fluid inclusions for microbial methanogenesis in the early Archaean era," *Nature*, vol. 440, no. 7083, pp. 516–519, 2006.

[53] B. Sherwood Lollar, S. K. Frape, S. M. Weise, P. Fritz, S. A. Macko, and J. A. Welhan, "Abiogenic methanogenesis in crystalline rocks," *Geochimica et Cosmochimica Acta*, vol. 57, no. 23–24, pp. 5087–5097, 1993.

[54] B. Sherwood Lollar, G. Lacrampe-Couloume, K. Voglesonger, T. C. Onstott, L. M. Pratt, and G. F. Slater, "Isotopic signatures of CH_4 and higher hydrocarbon gases from Precambrian Shield sites: A model for abiogenic polymerization of

hydrocarbons," *Geochimica et Cosmochimica Acta*, vol. 72, no. 19, pp. 4778–4795, 2008.

[55] J. Y. Lee, K. Marti, J. P. Severinghaus et al., "A redetermination of the isotopic abundances of atmospheric Ar," *Geochimica et Cosmochimica Acta*, vol. 70, no. 17, pp. 4507–4512, 2006.

[56] T. Staudacher and C. J. Allegre, "Recycling of oceanic crust and sediments: the noble gas subduction barrier," *Earth and Planetary Science Letters*, vol. 89, no. 2, pp. 173–183, 1988.

[57] J. Yamamoto, I. Kaneoka, S.'. Nakai, H. Kagi, V. S. Prikhod'ko, and S. Arai, "Evidence for subduction-related components in the subcontinental mantle from low $^{3}He/^{4}He$ and $^{40}Ar/^{36}Ar$ ratio in mantle xenoliths from Far Eastern Russia," *Chemical Geology*, vol. 207, no. 3–4, pp. 237–259, 2004.

[58] G. Czuppon, T. Matsumoto, M. R. Handler, and J. I. Matsuda, "Noble gases in spinel peridotite xenoliths from Mt Quincan, North Queensland, Australia: undisturbed MORB-type noble gases in the subcontinental lithospheric mantle," *Chemical Geology*, vol. 266, no. 1–2, pp. 19–28, 2009.

[59] S. Mukhopadhyay, "Early differentiation and volatile accretion recorded in deep-mantle neon and xenon," *Nature*, vol. 486, no. 7401, pp. 101–104, 2012.

[60] N. A. Starkey, F. M. Stuart, R. M. Ellam, J. G. Fitton, S. Basu, and L. M. Larsen, "Helium isotopes in early Iceland plume picrites: Constraints on the composition of high $^{3}He/^{4}He$ mantle," *Earth and Planetary Science Letters*, vol. 277, no. 1-2, pp. 91–100, 2009.

[61] D. Chavrit, R. Burgess, H. Sumino et al., "The contribution of hydrothermally altered ocean crust to the mantle halogen and noble gas cycles," *Geochimica et Cosmochimica Acta*, vol. 183, pp. 106–124, 2016.

[62] Z. Cheng, Z. Zhang, T. Hou et al., "Decoupling of Mg–C and Sr–Nd–O isotopes traces the role of recycled carbon in magnesiocarbonatites from the Tarim Large Igneous Province," *Geochimica et Cosmochimica Acta*, vol. 202, pp. 159–178, 2017.

[63] M. Schidlowski, "A 3,800-million-year isotopic record of life from carbon in sedimentary rocks," *Nature*, vol. 333, no. 6171, pp. 313–318, 1988.

[64] C. G. Macpherson, D. R. Hilton, J. M. D. Day, D. Lowry, and K. Gronvold, "High-$^{3}He/^{4}He$, depleted mantle and low-$\delta^{18}O$, recycled oceanic lithosphere in the source of central Iceland magmatism," *Earth and Planetary Science Letters*, vol. 233, no. 3–4, pp. 411–427, 2005.

[65] S. Shilobreeva, I. Martinez, V. Busigny, P. Agrinier, and C. Laverne, "Insights into C and H storage in the altered oceanic crust: Results from ODP/IODP Hole 1256D," *Geochimica et Cosmochimica Acta*, vol. 75, no. 9, pp. 2237–2255, 2011.